5
NSI effects on tripartite entanglement in neutrino oscillations

This chapter presents the findings of ref. [139]. In this study, we investigate the impact of new physics on different measures of tripartite entanglement within the context of three-flavor neutrino oscillations. Quantum correlations are a multifaceted concept within the domain of quantum mechanics, and they cannot be fully described by a single quantity or measure. Instead, there are various aspects used to characterize these correlations. One of the most famous and intriguing facets of quantum correlations is entanglement. Entanglement serves as a fundamental resource in various quantum information processing tasks, including quantum teleportation [283] and quantum cryptography [282]. Importantly, entanglement is not a single-valued quantity; rather, there are numerous methods to quantify it. These quantification approaches include Entanglement of Formation [132, 133], Concurrence [134, 135], and Negativity [136, 137]. The entanglement of formation is a fundamental concept in the realm of quantum physics. It is defined as the von Neumann entropy of the reduced density matrix, as perceived by any of the three parties involved, namely A, B, or C. In simpler terms, it quantifies the minimum level of entanglement that must be shared among three parties to create a specified quantum state. An intriguing property of EOF is that its value is only zero when the quantum state is separable, underlining its usefulness in identifying entanglement.

Concurrence is another widely used measure for quantifying entanglement. It was introduced as a more tractable alternative to EOF, which involves a minimization step in its definition, making analytical analysis challenging. Concurrence signifies the maximum potential entanglement attainable for a given set of eigenvalues of the density matrix. Its values range between 0 and 1, with 1 indicating maximal entanglement. Initially, concurrence was defined exclusively for two-qubit states, but recent work by Guo and Gour has extended its applicability to three-qubit states [135]. Negativity is yet another measure used to characterize entanglement. It is defined as the sum of the absolute values of the negative eigenvalues of the partially transposed density matrix. One of its significant advantages is its applicability to mixed quantum states, where other measures are more suitable for pure states. Notably, EOF, defined in terms of von Neumann entropy, may not effectively capture entanglement in mixed states since each subsystem possesses non-zero entropy, even in the absence of entanglement. In comparison, negativity provides a more comprehensive characterization of entanglement in mixed states. Therefore, negativity, while a valuable tool, is generally a weaker measure when compared to EOF and concurrence. In this work, we focus on examining the influence of NSI on different measures of entanglement, such as EOF, concurrence, and negativity. We investigate the effects of NSI across a spectrum of experimental set-ups, spanning various experimental configurations, including reactors and accelerators such as Daya Bay [130, 131], JUNO [129], KamLAND [187], T2K [127], MINOS [125], and DUNE [124], all within the framework of three-flavor neutrino oscillations.

This chapter is structured as follows: section 5.1 delves into the discussion of tripartite

entanglement measures. Next, section 5.2 outlines the formalization of our study in conjunction with matter and NSI. Subsequently, section 5.3 presents our findings, and section 5.4 encapsulates our concluding remarks.

5.1 Entanglement measures

In this section, we delve into the description of tripartite entanglement measures, both in terms of probabilities and through the lens of reduced density matrices. In the tripartite entanglement scenario, the quantum states of three particles are intertwined in a manner where the state of any one particle cannot be explained separately from the states of the other two particles. This implies that measurements conducted on one particle can immediately affect the states of the other two particles, irrespective of the spatial separation between them. In the realm of neutrino oscillations, the notion of tripartite entanglement emerges from blending the three flavor eigenstates with the underlying mass eigenstates. This combination results in quantum superposition in which the state of one flavor becomes intricately connected with the others, surpassing their distinct identities. After suitable approximations, we can also consider a two-flavor neutrino oscillation scenario that can allow us to quantify entanglement in terms of bipartite quantum correlation measures involving two parties. These bipartite measures provide a concise framework for understanding the correlation between two flavor states [114, 115]. However, in this work, we focus on tripartite entanglement. In this section, we will provide a succinct overview of some of the tripartite entanglement quantum correlation measures that have been employed in this study.

Entanglement of Formation: Two quantum systems, A and B, are represented by a density matrix. We can decompose this density matrix into all possible pure-state ensembles $|\psi_i\rangle$ and their associated probabilities p_i. Mathematically, this can be expressed as

$$\rho = \sum_i p_i \left|\psi_i\right\rangle \left\langle\psi_i\right|, \tag{5.1}$$

where ρ denotes the density matrix for composite systems A and B, $|\psi_i\rangle$ denotes the pure states in the ensemble, and p_i denotes the corresponding probabilities. The completeness of the ensemble is ensured by the requirement that the sum of the probabilities over all pure states equal to one. This decomposition facilitates the representation of the density matrix in terms of its constituent pure states and their probabilities, thereby providing a more detailed understanding of the quantum correlations inherent in the system.

To quantify the entanglement within subsystems A or B, the EOF is defined for each pure state within the ensemble as:

$$EOF(|\psi_i\rangle) = -Tr(\rho_A \log_2 \rho_A) = -Tr(\rho_B \log_2 \rho_B), \tag{5.2}$$

here $\rho_{A(B)}$ represents the partial trace of the density matrix ρ, yielding the reduced density matrix of subsystem A (B). The entanglement characterized by the EOF can then be generalized to encompass an arbitrary tripartite pure state $\rho_{ABC}(t)$. In this context, the EOF for such a tripartite state is often defined as follows [133]

$$EOF(\rho_{ABC}(t)) = \frac{1}{2}[S(\rho_A) + S(\rho_B) + S(\rho_C)], \tag{5.3}$$

where ρ_A, ρ_B and ρ_C are reduced density matrices which are $\rho_A = Tr_{BC}(\rho_{ABC}(t))$, $\rho_B = Tr_{AC}(\rho_{ABC}(t))$ and $\rho_C = Tr_{AB}(\rho_{ABC}(t))$. Further $S_(\rho_A)$, $S_(\rho_B)$ and $S_(\rho_C)$ are von Neumann entropies defined as $S_(\rho_A) = -Tr(\rho_A \log \rho_A)$ and same with $S_(\rho_B)$ and $S_(\rho_C)$.

EOF in terms of survival and oscillation probabilities for vacuum can be presented as follows [94]:

$$\begin{aligned} EOF^{\alpha} = -\frac{1}{2}[&P_{\alpha e}\log_2 P_{\alpha e} + P_{\alpha\mu}\log_2 P_{\alpha\mu} + P_{\alpha\tau}\log_2 P_{\alpha\tau} \\ &+(P_{\alpha\mu}+P_{\alpha\tau})\log_2(P_{\alpha\mu}+P_{\alpha\tau}) \\ &+(P_{\alpha e}+P_{\alpha\tau})\log_2(P_{\alpha e}+P_{\alpha\tau}) \\ &+(P_{\alpha\mu}+P_{\alpha e})\log_2(P_{\alpha\mu}+P_{\alpha e})]. \end{aligned} \tag{5.4}$$

Here $\alpha = e, \mu, \tau$, representing the initial flavor state of the neutrino.

Concurrence: Originally introduced for two-qubit states by Wootters in 1998 [134], the concurrence has traditionally been a measure of entanglement limited to such systems. However, a recent study has demonstrated that the concept of concurrence can be extended to quantify entanglement in three-qubit states as well. This expansion of the concurrence's applicability represents a significant advancement in our understanding of entanglement in more complex quantum systems. [135]

$$C(\rho_{ABC}) = [3 - Tr(\rho_A)^2 - Tr(\rho_B)^2 - Tr(\rho_C)^2]^{\frac{1}{2}}, \tag{5.5}$$

where $\rho_A = Tr_{BC}(\rho_{ABC}(t))$, $\rho_B = Tr_{AC}(\rho_{ABC}(t))$ and $\rho_C = Tr_{AB}(\rho_{ABC}(t))$.

For oscillating neutrinos, the concurrence for vacuum can be expressed in terms of oscillation and survival probabilities as [94]

$$C^{\alpha} = \sqrt{3 - 3P_S - 2P_{\alpha\mu}P_{\alpha\tau} - 2P_{\alpha e}(P_{\alpha\mu}+P_{\alpha\tau})}, \tag{5.6}$$

where P_S is the sum of the square of probabilities, and it is defined as $(P_{\alpha e}^2 + P_{\alpha\mu}^2 + P_{\alpha\tau}^2)$.

Negativity: In an alternative approach to quantifying entanglement within a system, the concept of negativity (N) is employed [136, 137]. It is defined as

$$N = (N_{A-BC}N_{B-CA}N_{C-AB})^{\frac{1}{3}}, \tag{5.7}$$

where $N_{A-BC} = -\sum_i \lambda_i^A$, $N_{B-CA} = -\sum_j \lambda_j^B$ and $N_{C-AB} = -\sum_k \lambda_k^C$. Here λ_i^A, λ_j^B and λ_k^C are negative eigenvalues of $\rho_{ABC}^{T_\alpha}(t)$, which is partial transpose of matrix $\rho_{ABC}(t)$.

In terms of survival and oscillation probabilities, negativity is given as [94]:

$$N^{\alpha} = [\sqrt{P_{\alpha e}}\sqrt{P_{\alpha\mu}+P_{\alpha\tau}}\sqrt{P_{\alpha e}}\sqrt{P_{\alpha\mu}}\sqrt{P_{\alpha e}+P_{\alpha\mu}}\sqrt{P_{\alpha\tau}}]^{\frac{1}{3}}. \tag{5.8}$$

In the next section, we will discuss formalism, by which we can compute the measures discussed in this section.

5.2 Formalism

The three-flavor neutrino oscillation is discussed in great detail in chapter 2 in sections 2.3 and 2.4. For better readability, we are providing concise details here. In the formalism of three-flavor neutrino oscillations, the flavor states ν_e, ν_μ, and ν_τ are expressed as a combination of the mass eigenstates ν_1, ν_2, and ν_3. This relationship is represented by the eq. $|\nu_\alpha\rangle = \sum_i U\,|\nu_i\rangle$, where U is PMNS matrix are given by

$$\begin{pmatrix} c_{12}c_{13} & s_{12}c_{13} & s_{13}e^{-\iota\delta} \\ -s_{12}c_{23} - c_{12}s_{13}s_{23}e^{\iota\delta} & c_{12}c_{23} - s_{12}s_{13}s_{23}e^{\iota\delta} & c_{13}s_{23} \\ s_{12}s_{23} - c_{12}s_{13}c_{23}e^{\iota\delta} & -c_{12}s_{23} - s_{12}s_{13}c_{23}e^{\iota\delta} & c_{13}c_{23} \end{pmatrix}. \tag{5.9}$$

These matrix elements are parameterized by mixing angles, such as θ_{12}, θ_{13}, and θ_{23}, which describe the blending of different flavor components. Here $s_{ij} = \sin\theta_{ij}$ and $c_{ij} = \cos\theta_{ij}$. Additionally, there exists a CP-violating phase, typically denoted as δ_{CP}, which introduces the violation of combined charge conjugation and parity symmetries. While not included in the original matrix, this phase becomes relevant when studying CP violation in neutrino oscillations. In this work, for the sake of simplicity, we will disregard the CP-violating phase.

Neutrinos, as they traverse through matter, can engage in interactions; these interactions can have consequences for the characteristic flavor oscillation pattern. When neutrinos are inside a medium, and these interactions are considered, the Hamiltonian of the SO in the matter can be expressed as follows [266]

$$\mathcal{H}_m = \mathcal{H}_{vac} + \mathcal{H}_{mat} = \begin{pmatrix} E_1 & 0 & 0 \\ 0 & E_2 & 0 \\ 0 & 0 & E_3 \end{pmatrix} + U^\dagger \begin{pmatrix} A & 0 & 0 \\ 0 & 0 & 0 \\ 0 & 0 & 0 \end{pmatrix} U. \tag{5.10}$$

Here, the Hamiltonian for neutrino oscillations in vacuum is denoted as $\mathcal{H}_{vac}$, while $\mathcal{H}_{mat}$ represents the Hamiltonian accounting for oscillations in the presence of matter. Additionally, $A = \pm\sqrt{2}G_F N_e$ is the matter potential is around 10^{-13} eV, corresponding to Earth's matter density of $\rho = 2.8$ gm/cc. Notably, the sign of the matter potential hinges on the type of neutrinos being considered. Specifically, for neutrinos, the matter potential is positive, whereas for antineutrinos, it is negative.

The impact of NSI is expected to play a subheading role in neutrino flavor oscillations. These NSI effects, affecting both CC and NC interactions, can be incorporated by means of four-fermion dimension-6 operators. The Hamiltonian in the presence of NSI will be $\mathcal{H}_{tot} = \mathcal{H}_{vac} + \mathcal{H}_{mat} + \mathcal{H}_{NSI}$, which can be written as

$$\mathcal{H}_{tot} = \begin{pmatrix} E_1 & 0 & 0 \\ 0 & E_2 & 0 \\ 0 & 0 & E_3 \end{pmatrix} + U^\dagger A \begin{pmatrix} 1+\epsilon_{ee}(x) & \epsilon_{e\mu}(x) & \epsilon_{e\tau}(x) \\ \epsilon_{\mu e}(x) & \epsilon_{\mu\mu}(x) & \epsilon_{\mu\tau}(x) \\ \epsilon_{\tau e}(x) & \epsilon_{\tau\mu}(x) & \epsilon_{\tau\tau}(x) \end{pmatrix} U. \tag{5.11}$$

The $\epsilon_{\alpha\beta}(x)$ are NSI parameters, where $\alpha, \beta = e, \mu, \tau$. NSI parameters can take on both real and complex values. From the Hermiticity condition, $\epsilon_{\alpha\beta} = \epsilon_{\beta\alpha}*$ i.e., $\epsilon_{\alpha\beta}$ is equal to the complex conjugate of $\epsilon_{\beta\alpha}$. For real NSI parameters, however, the condition $\epsilon_{\alpha\beta} = \epsilon_{\beta\alpha}$ holds, ensuring symmetry. NSI parameters are discussed earlier in subsection 2.4.1 in great detail.

In the ultra-relativistic limit, the time evolution operator for a neutrino mass eigenstate is given by $U_m(L) = e^{-i\mathcal{H}_{tot}L}$. In the context of three-flavor neutrino oscillations, the evolution operator $U_m(L)$ can be expressed as follows [202]

$$U_m(L) = e^{-i\mathcal{H}_{tot}L} = \phi\, e^{-iLT}\phi \sum_{a=1}^{3} e^{-iL\lambda_a} \frac{1}{3\lambda_a^2 + c_1} \left[(\lambda_a^2 + c_1)I + \lambda_a T + T^2\right]. \tag{5.12}$$

Here ϕ is a complex phase factor, which is defined as $\phi = e^{-\iota L(trH_{tot})/3}$, where L is the length between the source and detector, while H_{tot} is the total Hamiltonian, which accounts for vacuum, matter, and NSI effects. The coefficient c_1 is real, which is defined as the multiplication of the determinant of T and trace of T^{-1}. λ_1, λ_2 and λ_3 are the eigenvalues of the matrix T, which is given as

$$T \equiv \mathcal{H}_{tot} - (trH_{tot})I/3 = \begin{pmatrix} T_{11} & T_{12} & T_{13} \\ T_{21} & T_{22} & T_{23} \\ T_{31} & T_{32} & T_{33} \end{pmatrix}. \tag{5.13}$$

The evolution operator $U_f(L)$, which operates in the flavor basis, can be computed as $U_f(L) = U^\dagger U_m(L) U$. This evolution operator in the flavor basis is essential for calculating the probabilities of neutrino oscillations. To calculate the probabilities, we focus on the matrix elements of the evolution operator in the flavor basis. The probabilities are expressed as follows

$$\tilde{P}_{\alpha\beta} \equiv |A_{\alpha\beta}|^2 = |\langle\beta| U_f(L) |\alpha\rangle|^2 . \tag{5.14}$$

In this context, $\tilde{P}_{\alpha\beta}$ represents the probability of neutrino oscillation in the presence of NSI. In the formalism described above, the mass evolution operator $U_m(L)$ depends on the Hamiltonian of the system. When considering vacuum oscillations, the operator $U_m(L)$ is constructed using the vacuum Hamiltonian $\mathcal{H}_{vac}$. On the other hand, when neutrinos interact with matter, the operator $U_m(L)$ involves the matter Hamiltonian $\mathcal{H}_m$, which accounts for both vacuum and matter effects. In the presence of NSI, the operator $U_m(L)$ is based on the total Hamiltonian $\mathcal{H}_{tot}$, which encompasses contributions from vacuum, matter, and NSI. The choice of the appropriate Hamiltonian depends on the specific context being considered, whether it's vacuum, matter, or the inclusion of NSI effects.

In the context of the relativistic limit, neutrino flavor states are treated as individual modes, which we discussed in subsection 3.4.1 in detail for the three-qubit system. We can derive the time evolution for the tripartite quantum state as follows:

$$|\nu_\alpha(t)\rangle = \bar{U}_{\alpha e}(t) |100\rangle_{e\mu\tau} + \bar{U}_{\alpha\mu}(t) |010\rangle_{e\mu\tau} + \bar{U}_{\alpha\tau}(t) |001\rangle_{e\mu\tau} . \tag{5.15}$$

Here, considering the flavor state α at the initial time $t = 0$. For the state described in eq. 5.15, denoted as $\rho^\alpha_{ABC}(t) = |\nu_\alpha(t)\rangle \langle\nu_\alpha(t)|$, the density matrix is expressed as

$$\rho^\alpha_{ABC}(t) = \begin{pmatrix} 0 & 0 & 0 & 0 & 0 & 0 & 0 & 0 \\ 0 & \rho^\alpha_{22} & \rho^\alpha_{23} & 0 & \rho^\alpha_{25} & 0 & 0 & 0 \\ 0 & \rho^\alpha_{32} & \rho^\alpha_{33} & 0 & \rho^\alpha_{35} & 0 & 0 & 0 \\ 0 & 0 & 0 & 0 & 0 & 0 & 0 & 0 \\ 0 & \rho^\alpha_{52} & \rho^\alpha_{53} & 0 & \rho^\alpha_{55} & 0 & 0 & 0 \\ 0 & 0 & 0 & 0 & 0 & 0 & 0 & 0 \\ 0 & 0 & 0 & 0 & 0 & 0 & 0 & 0 \\ 0 & 0 & 0 & 0 & 0 & 0 & 0 & 0 \end{pmatrix}, \tag{5.16}$$

where the elements of this matrix can be written as

$$\begin{aligned} &\rho^\alpha_{22} = \left|\bar{U}_{\alpha\tau}(t)\right|^2 ; \rho^\alpha_{23} = \bar{U}_{\alpha\tau}(t)\bar{U}^*_{\alpha\mu}(t); \rho^\alpha_{25} = \bar{U}_{\alpha\tau}(t)\bar{U}^*_{\alpha e}(t); \\ &\rho^\alpha_{32} = \bar{U}_{\alpha\mu}(t)\bar{U}^*_{\alpha\tau}(t); \rho^\alpha_{33} = \left|\bar{U}_{\alpha\mu}(t)\right|^2 ; \rho^\alpha_{35} = \bar{U}_{\alpha\mu}(t)\bar{U}^*_{\alpha e}(t); \\ &\rho^\alpha_{52} = \bar{U}_{\alpha e}(t)\bar{U}^*_{\alpha\tau}(t); \rho^\alpha_{53} = \bar{U}_{\alpha e}(t)\bar{U}^*_{\alpha\mu}(t); \rho^\alpha_{55} = \left|\bar{U}_{\alpha e}(t)\right|^2 . \end{aligned} \tag{5.17}$$

The associated probabilities are as follows: $P_{\alpha e}(t) = \left|\bar{U}_{\alpha e}(t)\right|^2$ and $P_{\alpha\mu}(t) = \left|\bar{U}_{\alpha\mu}(t)\right|^2$. In the context of the ultra-relativistic limit, where length is approximately equal to time ($L \equiv t$), and when the energy difference $E_i - E_j$ is considerably smaller compared to the neutrino energy E, we can approximate it as $E_i - Ej \approx \Delta m^2_{ij}/2E$. Using the above density matrix, we can compute entanglement measures.

5.3 Results and Discussion

In this section, we delve into an exploration of how NSI affects tripartite entanglement measures within a three-flavor neutrino system. We focus on analyzing prominent entanglement measures, including entanglement of formation, concurrence, and negativity.

Table 5.1.: Standard neutrino oscillation parameters [335]

Parameters	Best fit$\pm 1\sigma$
θ_{12}^o	34.3 ± 1.0
θ_{13}^o	$8.58^{+0.11}_{-0.15}$
θ_{23}^o	$48.79^{+0.93}_{-1.25}$
$\Delta m^2_{21} \times 10^{-5}\,(\mathrm{eV}^2)$	$7.5^{+0.22}_{-0.20}$
$\Delta m^2_{31} \times 10^{-3}\,(\mathrm{eV}^2)$	$2.56^{+0.03}_{-0.04}$

Table 5.2.: NSI parameters [267] are given here, and these parameters are assumed to be real. The NSI upper limits have been used to generate the NSI plots.

NSI Parameters	Range (1σ)	Range (2σ)
$\epsilon^{\oplus}_{ee}$	[-0.30, 0.20] $\oplus$ [0.95, 1.3]	[-1.00, 1.4]
$\epsilon^{\oplus}_{e\mu}$	[-0.12, 0.011]	[-0.20, 0.09]
$\epsilon^{\oplus}_{e\tau}$	[-0.16, 0.083]	[-0.24, 0.30]
$\epsilon^{\oplus}_{\mu\mu}$	[-0.43, 0.14] $\oplus$ [0.91, 1.3]	[-0.80, 1.4]
$\epsilon^{\oplus}_{\mu\tau}$	[-0.047, 0.012]	[-0.021,0.021]
$\epsilon^{\oplus}_{\tau\tau}$	[-0.43, 0.21] $\oplus$ [0.83, 1.3]	[-0.85, 1.4]

Our examination encompasses various experimental setups, specifically those involving reactors and accelerators. Through detailed analysis, we aim to discern the impact of NSI on the entanglement characteristics of neutrinos, shedding light on the intricate interplay between quantum correlations and particle interactions. We consider the following reactor and accelerator experimental setups:

- Daya Bay ($L \approx 2$ km, $E \approx 0.8 - 6$ MeV) [130, 131],
- JUNO ($L \approx 53$ km, $E \approx 1 - 8$ MeV) [128, 129],
- KamLAND ($L \approx 180$ km, $E \approx 1 - 16$ MeV) [187],
- T2K ($L \approx 295$ km, $E \approx 0 - 6$ GeV) [126, 127],
- MINOS ($L \approx 735$ km, $E \approx 1 - 10$ GeV) [125],
- DUNE ($L \approx 1300$ km, $E \approx 1 - 14$ GeV) [123, 124].

The standard neutrino oscillation parameters are presented in table 5.1, while the NSI parameters are provided in table 5.2. These tables pertain to the framework of three-flavor neutrino oscillations. In the context of reactor experiments, the initial neutrino is considered to be the antineutrino $\bar{\nu_e}$, whereas for accelerator experiments, the initial neutrino is denoted as ν_μ.

Figure 5.1 depicts the probabilities for NSI relative to the SO matter effect for the experimental configurations. As all the entanglement measures are expressed in terms of probabilities, we studied the effect of NSI on probabilities. In reactor experiments, where the initial neutrino state is ν_e, the probabilities P_{ee}, $P_{e\mu}$, and $P_{e\tau}$ are plotted. Conversely, in accelerator experiments, where ν_μ is the initial neutrino state, the probabilities $P_{\mu e}$, $P_{\mu\mu}$, and $P_{\mu\tau}$ are illustrated. The baseline of the experiments amplifies their sensitivity to NSI effects; a longer baseline results in a more pronounced influence on the probabilities. In reactor experiments, when P_{ee} is enhanced due to

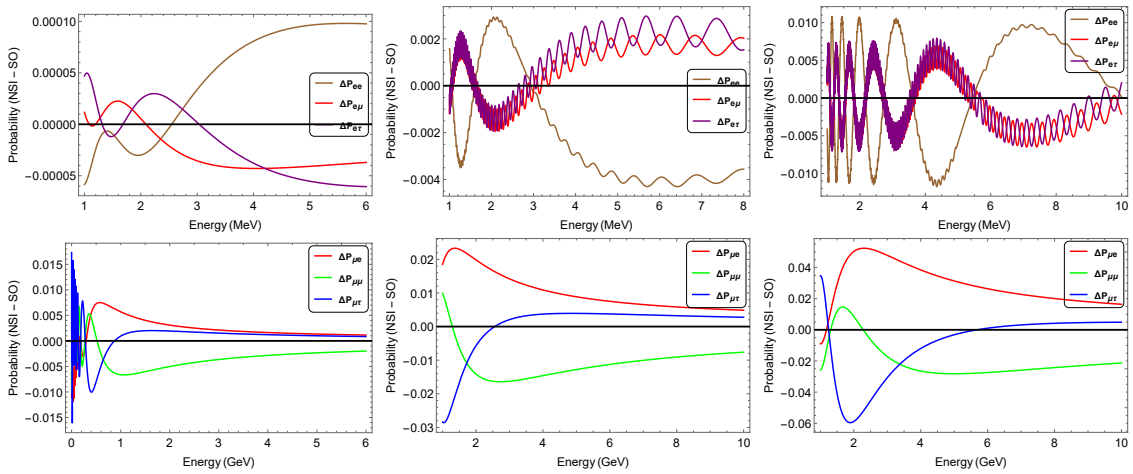

Figure 5.1.: Showing variation of probabilities for (NSI−SO) scenario with neutrino energies for reactor experiments in the upper panel, i.e., Daya Bay (left), JUNO (center), KamLAND (right) and for the accelerator in the lower panel, i.e., T2K (left), MINOS (center), DUNE (right). Color representation is brown for ΔP_{ee} , red for $\Delta P_{e\mu}$ or $\Delta P_{\mu e}$, purple for $\Delta P_{e\tau}$, green for $\Delta P_{\mu\mu}$ and blue for $\Delta P_{\mu\tau}$. Standard neutrino oscillation parameters and NSI parameters are given in table 5.1 and table 5.2, respectively.

NSI, it leads to a reduction in $P_{e\mu}$, $P_{e\tau}$, and vice versa. Overall, it is evident that the effect of NSI on probabilities is negligible in reactor experiments, so the same is expected in quantum correlation measures. In accelerator experiments, $P_{\mu e}$ exhibits slightly more dominance compared to $P_{\mu\mu}$ and $P_{\mu\tau}$.

Figure 5.2 illustrates the projected results for EoF, concurrence, and negativity in the context of different reactor neutrino oscillation experiments, namely Daya Bay, JUNO, and KamLAND. The right panel of each experiment showcases the differences in these measures, denoted as ΔEoF, ΔC, and ΔN, between the scenario with NSI and the SO in the matter scenario. This visual representation serves to emphasize the discernible distinctions between the two scenarios, facilitating a clearer understanding of the impact of NSI on entanglement measures. The left panel of the diagram clearly showcases a notable trend across all three assessed setups. For the JUNO and KamLAND configurations, the EoF stands out as a notably robust measure of entanglement. In contrast, for the Daya Bay setup, the concurrence exhibits higher values throughout the entire energy range under scrutiny. Conversely, negativity consistently demonstrates weaker values within this energy range. Significantly, this pattern remains consistent for both the matter SO scenario and the introduction of NSI. This finding underscores the enduring importance of both EoF and concurrence as potent indicators of entanglement, particularly in the context of neutrino oscillation experiments.

In the right panel of figure 5.2, it becomes evident that among the three entanglement measures, the negativity measure is the least influenced by the presence of NSI across all three reactor experimental configurations under consideration. Additionally, it is noteworthy that the impact of NSI is most subdued for the Daya Bay setup, whereas it is most pronounced for the KamLAND setup. This consistent trend holds true for all three entanglement measures. This observation can be attributed to the fact that the baseline distance is the greatest for the KamLAND configuration compared to the other two setups. The extended baseline enhances the sensitivity of the KamLAND setup to NSI effects, leading to a more pronounced influence on the entanglement measure. Overall, the effect of NSI is almost negligible in the reactor experiments. This result is also depicted in the left panel of figure 5.2 where the SO (dashed line) and NSI (solid line) curves

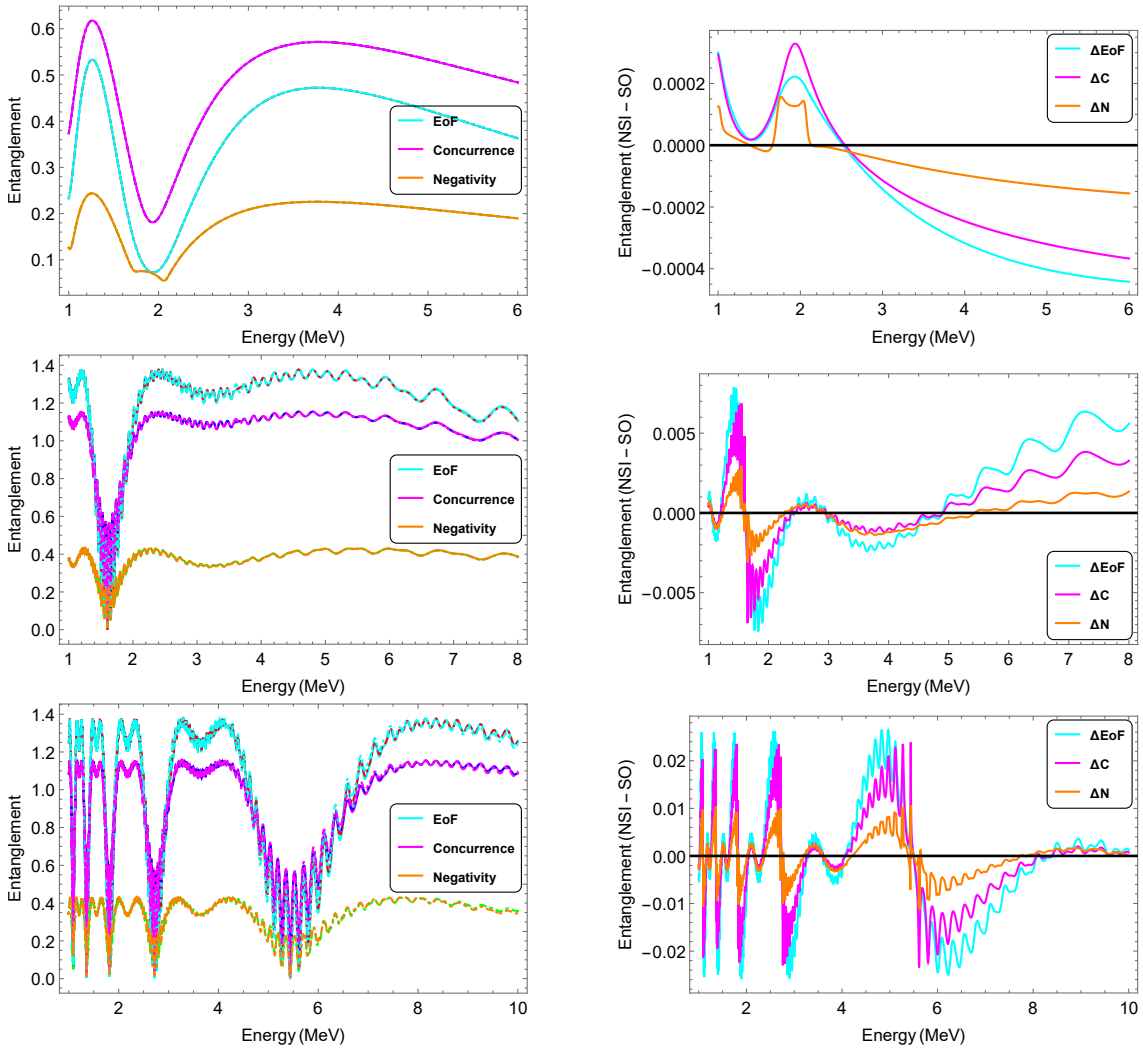

Figure 5.2.: The three panels depict the prediction of EOF, concurrence, and negativity for various reactor neutrino oscillation experimental setups, i.e., Daya Bay (upper), JUNO (middle), and KamLAND (lower). Oscillation and NSI parameters are the same as given in figure 5.1. Color representation follows cyan for EoF, magenta for concurrence, and orange for negativity. In the left panel, NSI is represented by solid lines, and the vacuum is represented by dot-dashed lines. The SO matter effect is represented by dot-dashed lines; color representation follows red for EoF, blue for concurrence, and green for negativity.

are the same, while in the right panel, we can observe that the NSI effect is almost negligible.

Figure 5.3 illustrates the analysis of the three entanglement metrics within accelerator experiments, specifically T2K, MINOS, and DUNE. In the left panel of the figure, it becomes evident that in the low-energy range, both EOF and concurrence can be regarded as robust measures of entanglement across all three experimental configurations, as their values closely align. However, in the high-energy domain, for T2K and MINOS experiments, concurrence exhibits slightly greater strength in comparison to EOF. Conversely, for the DUNE setup, the values of these two measures remain nearly identical, even for higher neutrino energy values. Similar to the reactor experimental setups considered, negativity consistently appears as a weaker measure for all three accelerator setups across the entire energy spectrum considered. Remarkably, these findings hold true for both matter SO and NSI interactions. The right panel of figure 5.3 provides a closer look at the impact of NSI, characterized by the difference between values in the presence of NSI and

SO matter interactions. Notably, the NSI effects are least pronounced for the T2K setup among all three configurations, while they are most prominent for the DUNE experiment. The MINOS experiment experiences moderate NSI effects. This discrepancy can be attributed to differences in the baseline length.

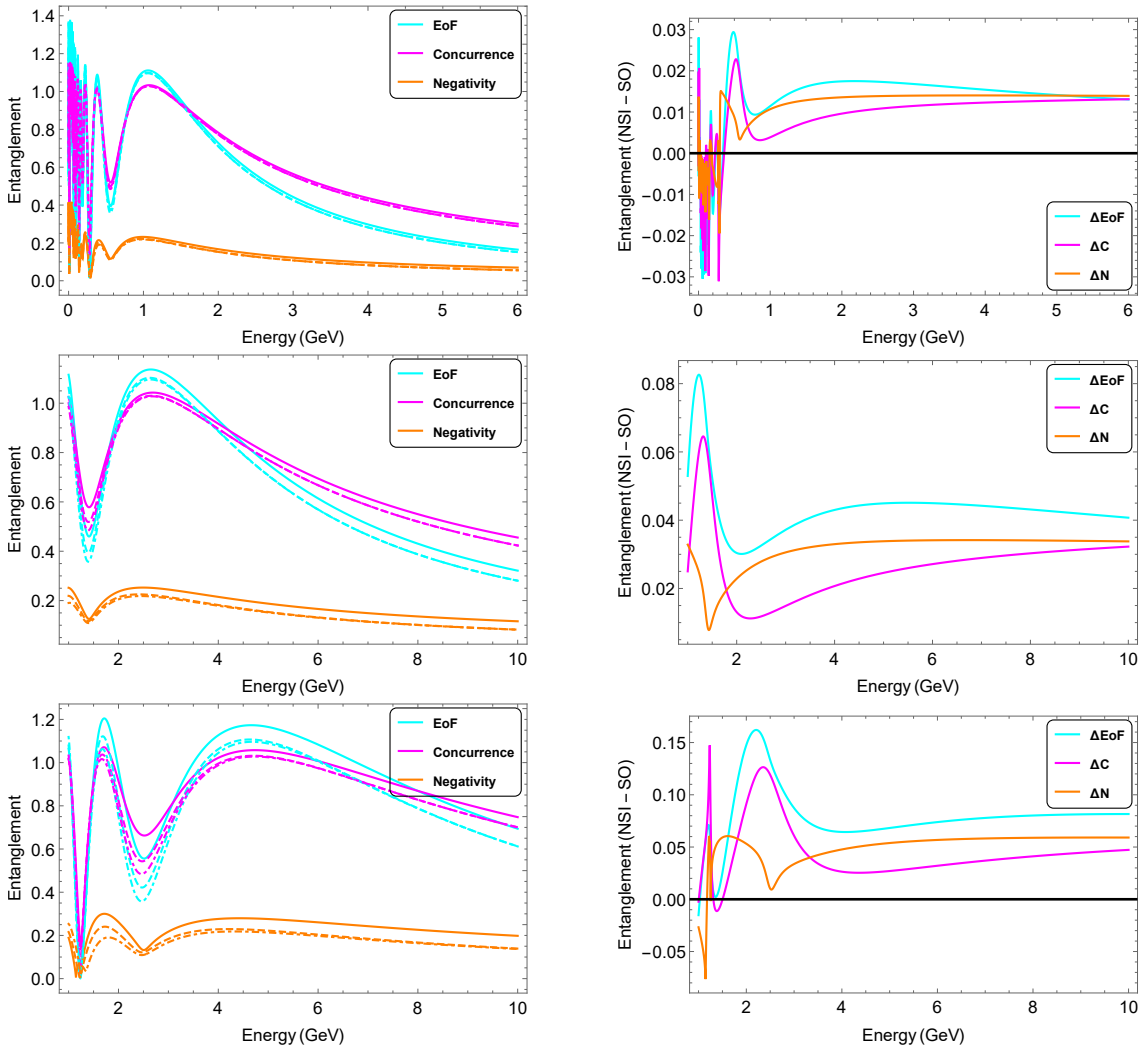

Figure 5.3.: The three panels depict the prediction of EOF, concurrence, and negativity for various accelerator neutrino oscillation experimental setups, i.e., T2K (upper), MINOS (middle), and DUNE (lower). Oscillation and NSI parameters are the same as given in figure 5.1. Colour representation follows cyan for EoF, magenta for concurrence, and orange for negativity. In the left panel, NSI is represented by solid lines, the SO matter effect is represented by dashed lines, and the vacuum is represented by dot-dashed lines.

In eq. 5.4, when NSI enhances $P_{\mu e}$ and reduces $\log_2 P_{\mu e}$, the overall effect is that the first three terms increase while the last three terms decrease, relative to the SO matter effect. The primary impact arises from the first three terms in eq. 5.4, leading to an increase in EoF for NSI. In eq. 5.6, the term $3(P_{\alpha e}^2 + P_{\alpha \mu}^2 + P_{\alpha \tau}^2)$ dominates and possesses a higher value for the SO matter effect compared to NSI, while the other terms have higher values for NSI than the matter effect. Conversely, in eq. 5.8, the dependency of negativity on $P_{\mu e}$ outweighs that on the other two probabilities, and the impact of other terms is less significant. Hence, the enhancement for NSI is more pronounced in negativity. At lower energy ranges, $P_{\mu e}$ and $\sqrt{P_{\mu e} + P_{\mu \mu}}$ increase while other factors decrease and exert greater dominance. Consequently, the overall effect of NSI is a decrease in this scenario.

At E $\approx$ 3 GeV, i.e., the energy corresponding to the maximum neutrino flux at DUNE, the overall strength of entanglement measures decreases while the impact of NSI is maximum on EOF and concurrence. Similarly, in MINOS, the energy at which the neutrino flux reaches its maximum is $\approx$ 3 GeV. At this energy, the strength of all three entanglement measures is maximum, and the NSI effect is moderate on all three measures. While in T2K, the energy value at which the neutrino flux is maximized is ≈ 0.6 GeV. A similar feature like DUNE appears here; the strength of entanglement measures decreases at this value, but the effect of NSI on measures is maximum here.

Overall, the effect of NSI is negligible in the T2K experiment as this is governed by oscillation in vacuum. This result is also depicted from the left panel of figure 5.3 where the SO (dashed line) and NSI (solid line) curves are almost the same, while in the right panel, we can observe that the NSI effect is very less as compared to other accelerator experiments. In contrast to the three considered reactor experimental setups, it's observed that for all three accelerator experiments, NSI effects have the least impact on concurrence compared to EOF and negativity, particularly in the moderate and high-energy range of neutrinos. Specifically, EOF exhibits the highest sensitivity to NSI for the MINOS and DUNE experimental setups, whereas, for T2K, the NSI effects remain nearly the same for both EOF and negativity. In the low-energy region, the trends align with those observed in the reactor experiments, indicating that NSI effects are more pronounced for the EOF and concurrence measures as compared to negativity.

DUNE is expected to refine the acceptable values of NSI parameters [337–341], thereby reducing the differences in the quantum correlations between the matter SO and NSI scenarios. Recently expected sensitivity on NC-NSI by DUNE is studied in [341]. We also calculated the effect of these NC-NSI parameters in DUNE for a conservative scenario on quantum correlation measures. After DUNE sensitivity is taken into account, the value of EOF and concurrence reduces by approximately 60%, while the value of negativity reduces by approximately 40% at peak values. For higher energy ranges, the value of EOF and negativity reduces by approximately 60%, while the value of concurrence reduces by approximately 55%.

The primary motive of this work was to study the impact of NSI on various entanglement measures. For this, we have obtained theoretical predictions of entanglement measures using the current bounds on NSI parameters. Based on these predictions, we have identified the maximum possible deviations in entanglement measures, which are allowed by the current data. However, as these measures are expressed in terms of probabilities, such as $P_{\mu e}$, $P_{\mu\mu}$ and $P_{\mu\tau}$, the experimental measurement of these measures will be possible only if these probabilities are measured accurately.

5.4 Conclusion

The impact of NSI on entanglement measures (EoF, concurrence, and negativity) is explored for three-flavor neutrino oscillation scenarios investigated in this study. This work is among the first to present a comprehensive comparative analysis of the behavior of various quantum entanglement measures under the influence of NSI. The analysis is conducted across six neutrino experiments: T2K, MINOS, DUNE, Daya Bay, JUNO, and KamLAND. Among these, DUNE, with the longest baseline, exhibits a more pronounced deviation towards NSI compared to MINOS and T2K. Reactor experiments display lower sensitivity towards NSI, with negativity exhibiting the least sensitivity among entanglement measures. In contrast, accelerator experiments demonstrate greater sensitivity to NSI. Despite entanglement of formation and concurrence being effective measures in accelerator experiments, negativity still exhibits higher sensitivity than concurrence towards NSI.